Available online at www.sciencedirect.com

ScienceDirect

Journal of Materiomics 1 (2015) 75–84

www.ceramsoc.com/en/

www.journals.elsevier.com/journal-of-materiomics/

Temperature dependent solubility of Yb in Yb–$CoSb_3$ skutterudite and its effect on preparation, optimization and lifetime of thermoelectrics

Yinglu Tang [a], Sinn-wen Chen [b], G. Jeffrey Snyder [a,*]

[a] Department of Applied Physics and Materials Science, California Institute of Technology, Pasadena, CA 91125, USA
[b] Department of Chemical Engineering, National Tsing Hua University, #101, Sec.2, Kuang-Fu Rd., Hsin-Chu 300, Taiwan, China

Received 14 January 2015; revised 19 January 2015; accepted 30 January 2015
Available online 1 April 2015

Abstract

Although filled skutterudites are actively being developed for automotive waste heat recovery the compositions considered available are limited. Typically synthesis conditions are chosen with slight excess filling element to produce filled skutterudites at the 'filling fraction limit', traditionally considered to be a single value that depends only on the elements involved (e.g. filling element, Co/Fe ratio). The filling fraction limit is often debated and thought perhaps to vary with processing method. This work opens up a new dimension of available compositions by showing that the 'filling fraction limit' is a thermodynamic quantity that for Yb varies by a factor of 5 depending on annealing temperature and nominal composition. As the filling element controls the electronic doping in these semiconductors this study not only enables optimization of thermoelectric properties using thermodynamic control rather than non-equilibrium processing conditions (reaching $zT = 1.3$ at 850 K without nanostructures) but it also predicts dopant precipitation effects after extended use. The novel phase diagram approach used here should be easily applied to other ternary thermoelectric materials to uncover similar phenomena. Thus skutterudite material with the optimized thermoelectric composition can be produced from a range of nominal compositions with appropriate annealing.

Keywords: Skutterudites; Temperature dependent solubility; Thermoelectric; Optimization

1. Introduction

Thermoelectric materials can play a role in the solution for the world's increasing demand for energy with their ability to directly convert unused waste heat into electricity. The thermoelectric performance of materials is characterized by the dimensionless figure of merit, $zT = S^2\sigma T/\kappa$, where S is the Seebeck coefficient, σ is the electrical conductivity, T is the absolute temperature, and κ is the total thermal conductivity.

Filled skutterudites can have low thermal conductivity like a glass and high electrical conductivity like a crystal, which make them excellent thermoelectric materials according to the "phonon glass electron crystal" (PGEC) concept [1]. Among various kinds of filled skutterudite materials, Yb-doped skutterudites have shown good thermoelectric properties due to the heavy mass and small radius of the Yb atom compared to other fillers, and have been selected by many automotive companies, such as General Motors, as the most promising thermoelectric material for waste heat recovery [2]. Nolas et al. first reported a zT value of 1.0 for $Yb_{0.19}Co_4Sb_{12}$ at 600 K [3]. Composites containing Yb-filled $CoSb_3$ and well-distributed Yb_2O_3 particles were synthesized by Zhao et al. with zT of 1.3 for $Yb_{0.25}Co_4Sb_{12}/Yb_2O_3$ at 850 K [4]. Later zT of 1.3 for $Yb_{0.285}Co_4Sb_{12.268}$ at 800 K was reported by Li et al. [5].

Despite the good thermoelectric performance of Yb-doped skutterdites, there has been debate about the Yb solubility limit in skutterudite phase. Because of the size and chemical difference between Yb and Co or Sb atoms, substitution of Yb

* Corresponding author.
E-mail addresses: yttang@caltech.edu (Y. Tang), jsnyder@caltech.edu, jeff.snyder@northwestern.edu (G.J. Snyder).
Peer review under responsibility of The Chinese Ceramic Society.

http://dx.doi.org/10.1016/j.jmat.2015.03.008

for Co or Sb is not likely. Instead, the Yb atoms fit nicely into the void filling site, and thus the solubility limit discussed here corresponds to the filling fraction limit (FFL). Theoretically, the filling fraction limit was calculated by Mei et al. to be 0.30 for Yb at 0 K; Shi et al. studied the temperature dependence of filling fraction limits of fillers in $CoSb_3$ skutterudites using a plane-wave density functional method [6,7]. By combining the formation energy of inserting an impurity R into the intrinsic void of $CoSb_3$ and that of secondary phases RSb_2 and $CoSb_2$, it is found that theoretically the filling fraction limit has a linear dependence on temperature, with $x = 0.2$ when R = Yb at 1000 K which is close to the experimental value but the temperature dependence was not demonstrated experimentally. Dilley et al. synthesized $Yb_xCo_4Sb_{12}$ by induction heating samples at 1050 °C for 12 min then annealing at 600 °C for 35 h [8]. Lattice constant values were obtained from powder X-ray diffraction data and plotted against nominal x, from which Yb solubility limit about $x = 0.22$ was extrapolated. Xia et al. synthesized $Yb_xCo_4Sb_{12}$ with nominal x up to 0.4 by melting samples at 1077 °C for 10 h and subsequent annealing at 800 °C for 7 days and observed no impurity phases [9]. Addition of oxygen to the system results in less filling due to the formation of Yb oxides [10]. In addition to traditional preparation methods (melting and long-time annealing), non-equilibrium synthesis methods were also adopted and gave different solubility limits, such as $x = 0.29$ by melt-melt-spinning (MMS) method by Li et al. and $x = 0.5$ by ball milling by Yang et al. [5,11].

In this study, the equilibrium isothermal sections of the ternary phase diagram of Yb–Co–Sb system at various temperatures are proposed in the same way as for the Ga–Co–Sb system and In–Co–Sb system, which are based on knowledge of the related binary phase diagrams and the microstructure of the samples [12–16]. The filling fraction limit derived from the ternary phase diagram and especially its temperature dependence naturally explains the solubility debate and the confusion concerning the various reports of maximum solubility of Yb in the skutterudite phase. It also leads to a strategy to synthesize optimized, high zT material.

2. Methods

2.1. Sample synthesis

Nominal compositions: #1 $Yb_{0.25}Co_{3.8}Sb_{12.2}$, #2 $Yb_{0.25}Co_4Sb_{12}$, #3 $Yb_{0.25}Co_{4.2}Sb_{11.8}$, #4 $Yb_{0.5}Co_4Sb_{12}$, #5 $Yb_{0.5}Co_{4.2}Sb_{11.8}$, #6 $Yb_{0.5}Co_{3.9}Sb_{12.1}$, and #7 $Yb_{0.5}Co_{3.8}Sb_{12.2}$ were chosen based on preliminary phase diagram study with the knowledge of related binary phase diagrams. High-purity elements Co (99.95%, slug), Sb (99.9999%, shot), and Yb (99.9% , ingot) purchased from Alfa Aesar were used as raw materials. The samples were sealed in carbon coated fused silica tubes under vacuum. The silica tubes were heated slowly up to 1373 K in 12 h, held at this temperature for 12 h and then quenched in water to room temperature. Samples were then annealed at temperatures ranging from 773 K to 1073 K for 7 days. The resulting ingots were hand ground into fine powders and consolidated by rapid hot pressing at 973 K for 1 h under a pressure of about 60 MPa, yielding fully dense bulk samples [17]. High-density (>98% of the theoretical density of $CoSb_3$) was achieved in all hot pressed samples. Hot pressed samples were sealed in fused tubes under vacuum for further annealing at the same annealing temperatures as before for 7 days again to erase the temperature effect of the hot pressing process before thermoelectric properties were measured.

2.2. Structure characterization

Ingots after annealing were cut and characterized by room temperature powder X-ray diffraction (XRD), with data collected on a Panalytical X'Pert Pro diffractometer equipped with Cu Kα radiation to check phase purity and lattice constant. Microstructures of the annealed samples were checked with a ZEISS 1550VP Field Emission Scanning Electron Microscope (SEM). Quantitative elemental analyses of the annealed samples were performed with a JEOL JXA-8200 electron probe microanalysis (EPMA) using an accelerating voltage of 15 keV and a current of 25 nA in a WDS mode and averaged over 10 randomly selected locations in the skutterudite phase.

2.3. Thermoelectric transport property measurements

Electrical transport properties, including electrical conductivity (σ) and Seebeck coefficient (S) were measured using the ZEM-3 (ULVAC Co. Ltd.) apparatus under a helium atmosphere from 300 to 850 K. Thermal conductivity (κ) was calculated using $\kappa = dD_TC_P$, with the thermal diffusivity D_T measured along the cross-plane direction by the laser flash method (Netzsch LFA 457) under argon flow with the Cowan model plus pulse correction. The density of the samples was measured using geometrical method. The specific heat capacity C_P was determined using the Dulong–Petit law $C_p = 3k_B$ per atom throughout the temperature range 300K–850 K. The in-plane Hall coefficient (R_H) was measured using the Van der Pauw method in a magnetic field up to 2 T [18]. Hall carrier concentration (n) was then estimated to be equal to $1/R_He$, where e is the elementary charge. The Hall carrier mobility (μ_n) was calculated according to the relation $\mu_n = R_H\sigma$.

3. Results and discussion

Samples were prepared by a process of melting and quenching followed by annealing at various temperatures for one week in order to achieve the equilibrium state. Impurity phases were identified with XRD and confirmed with SEM analysis as described in the Methods section.

3.1. Skutterudite lattice expansion due to Yb filling

Lattice constants were derived from powder X-ray diffraction data and plotted against Yb actual content determined from EPMA, as shown in Fig. 1(a). We can see that there is a good linear relationship between the actual Yb content and lattice constant of the skutterudite phase, which agrees with the literature data and is consistent with Yb going

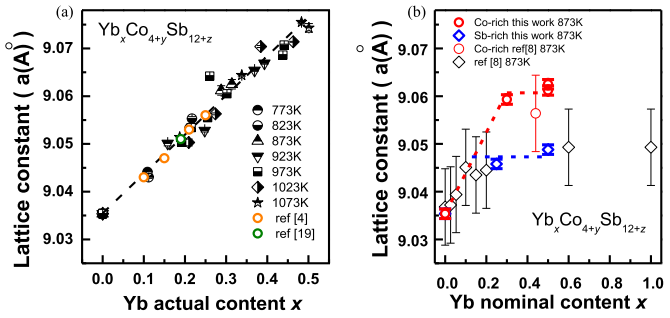

Fig. 1. (a) Dependence of lattice constant on the actual Yb content, x, in $Yb_xCo_{4+y}Sb_{12+z}$ for samples annealed at various temperatures in this study and samples in ref 4 and 19. (b) Dependence of the lattice constant on the nominal Yb content, x, in $Yb_xCo_{4+y}Sb_{12+z}$ for samples annealed at 873 K in this study and samples in ref 8. The red dashed line shows the increase of lattice constant followed by a plateau when x is larger than 0.30 in Co-rich samples which indicates the maximum filling fraction limit at 873 K (red point in Fig. 11a). The blue dashed line shows another plateau of lattice constant indicating another stable composition $Yb_{0.13}Co_4Sb_{12}$ (blue point in Fig. 11a) in Sb-rich samples.

into the same site across the whole range (up to $x = 0.5$), presumably the void site [4,19]. Lattice constants were also plotted against the nominal Yb content in order to compare with reference 8 in Fig. 1(b). The two plateaus of lattice constants in this study indicate there are two stable skutterudite compositions at 873 K (see Section 3.2 for explanation of stable compositions). The red dashed line shows the increase of lattice constant followed by a plateau when x is larger than 0.30 when the nominal composition is in a Co-rich three phase region. Here the Yb content in the skutterudite phase reaches the maximum filling fraction limit at 873 K (red point in Fig. 11(a)). The blue dashed line shows another plateau of lattice constant when the nominal composition is in a Sb-rich three phase region where the skutterudite phase has a stable composition with lower Yb content ($Yb_{0.13}Co_4Sb_{12}$, blue point in Fig. 11(a)). The lattice constants in this study (Fig. 1(b)) are well within the same range from reference 8. Moreover, for the $x = 0.44$ sample from reference 8 which has larger lattice constant than other samples, it has $YbSb_2$ and $CoSb_2$ impurities according to the XRD data, which agrees with our conclusion that the skutterudite phase with maximum filling fraction limit coexists with $CoSb_2$ and $YbSb_2$ and is thus in a Co-rich three phase region.

3.2. Stable compositions in ternary phase diagram system

The analysis of all samples is consistent with the proposed phase diagram for Yb-doped skutterudites shown in Fig. 2(a), which is based on the knowledge of the related binary phase diagrams [14–16]. Our experimental data suggest that the region of Yb solubility extends toward the void filling samples, $(Yb_{VF})_xCo_4Sb_{12}$, up to the maximum solubility point. For example, at 973 K the estimated maximum x value is 0.44 as shown in Fig. 2(a) (red point). When x exceeds 0.44, the sample $Yb_{0.5}Co_4Sb_{12}$ (empty orange rectangle surrounded by

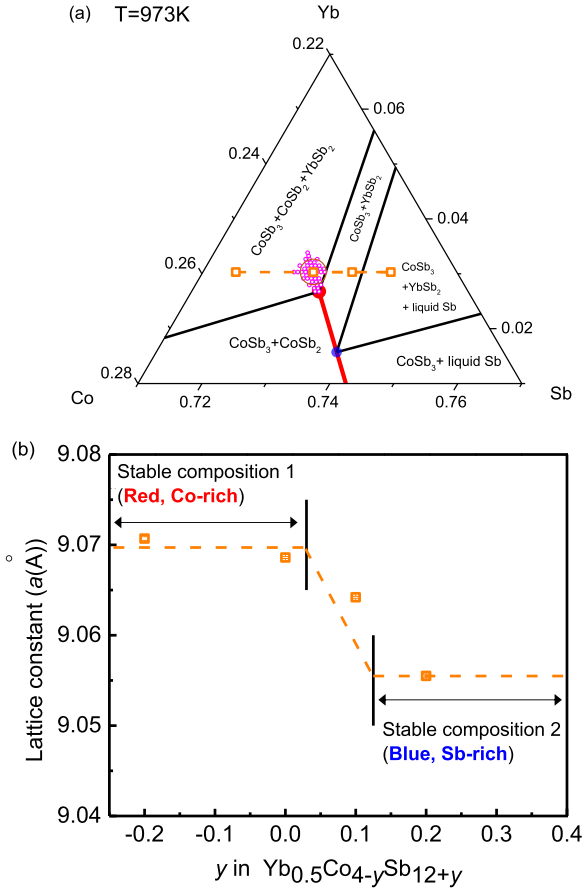

Fig. 2. (a) Magnified region of the isothermal section at 973 K near $CoSb_3$ of the Yb–Co–Sb ternary phase diagram system with two stable skutterudite compositions (red and blue points) and solubility line (red line). Scattered points (empty magenta circles) indicate possible synthesis error near the stable composition (red point) in the three phase region of $CoSb_3$, $CoSb_2$ and $YbSb_2$. (b) Dependence of the lattice constant derived from X-ray Diffraction data on the Co/Sb ratio for nominal compositions with the same Yb content $x = 0.5$ marked as empty orange rectangles in (a).

empty magenta circles) contains a skutterudite phase with Yb doping level around $x = 0.44$ and impurity phases $YbSb_2$ and $CoSb_2$. When the nominal composition with $x = 0.5$ is off the Co/Sb ratio of void filling samples $(Yb_{VF})_xCo_4Sb_{12}$ (being either Co-rich or Sb-rich), more impurity phases form in the samples.

When the nominal composition contains higher Yb content than its solubility limit, it is in a three phase region between $Yb_xCo_4Sb_{12}$, $YbSb_2$ and $CoSb_2$. According to the phase rule, there is $F = C - P + 0 = 3 - 3 = 0$ degree of freedom where C is the number of components, P the number of phases, and the 0 indicates both temperature and pressure are fixed. Thus the compositions of the three equilibrium phases in a three phase region are fixed and all the nominal compositions in this three phase region (such as all the scattered empty magenta circles in Fig. 2(a)) will produce the same skutterudite composition with the same actual Yb content (red point in Fig. 2(a)). This is indicated by a plateau of the lattice constant marked as *stable composition 1* from Fig. 2(b). At 973 K it was also confirmed by the EPMA measurements to be

$x = 0.44 \pm 0.01$($Yb_{0.44}Co_4Sb_{12}$) as shown in Table 1 in Supporting Material section.

When the nominal composition is slightly Sb-rich (for example $Yb_{0.5}Co_{3.9}Sb_{12.1}$ at 973 K), it moves into a two-phase region between $Yb_xCo_4Sb_{12}$ and $YbSb_2$. Due to the phase rule, the degree of freedom $F = C - P + 0 = 3 - 2 = 1$, which means that the compositions of phases at equilibrium in this two-phase region are not fixed, but vary depending on the exact starting composition within this region. As a result, the Yb content in the skutterudite phase decreases as the nominal composition becomes more Sb rich, which is confirmed by the decrease of lattice constant in Fig. 2(b).

However, when the nominal composition is even richer in Sb (for example $Yb_{0.5}Co_{3.8}Sb_{12.2}$ at 973 K), the nominal composition moves into another three-phase region between $Yb_xCo_4Sb_{12}$, $YbSb_2$ and liquid Sb. Thus the compositions of phases at equilibrium are fixed again and all the nominal compositions in this three phase region will produce the same skutterudite composition with the same actual Yb content ($Yb_{0.26}Co_4Sb_{12}$) albeit at a much lower Yb content (blue point in Fig. 2(a)). This was confirmed by a lower plateau of lattice constant marked as *stable composition 2* in Fig. 2(b) and the EPMA measurements confirmed this composition to be $x = 0.26 \pm 0.02$ as shown in Table 1 in Supporting Material section.

In the process of synthesizing samples, exact element control is not cost-practical and thus the influence of impurity elements from low-cost starting material will lead to variations in the Co/Sb ratio and Yb content as well, shown as scattered empty magenta circles in Fig. 2(a). If these scattered circles spill out of the three phase region and enter into the two phase region of $CoSb_3$ and $YbSb_2$, there will be a sharp decrease of Yb content in the skutterudite phase, resulting a sharp decrease in lattice constant as well, which is illustrated in Fig. 2(b). In order to have precise control of the Yb content and thus the carrier concentration in the skutterudite phase, nominal compositions can be easily designed to remain in a three phase region to make sure that the skutterudite phase has a stable composition. The existence of these stable compositions as well as their temperature dependence discussed in section 3.3 can thus be applied to facilitate the synthesis of optimized skutterudites for low-cost mass production.

This study also demonstrates that reaching a plateau of lattice constant does not necessarily imply reaching the solubility limit. In samples with even a slight Sb excess (depicted in Fig. 3(a)), increasing the nominal Yb content will lead to samples in the Sb-rich three phase region of $Yb_xCo_4Sb_{12}$, $YbSb_2$ and liquid Sb first, then samples in the two phase region of $Yb_xCo_4Sb_{12}$ and $YbSb_2$ before samples reaching the Co-rich three phase region of $Yb_xCo_4Sb_{12}$, $YbSb_2$ and $CoSb_2$. Thus the actual Yb content in Yb filled $CoSb_3$ as measured by the lattice constant of the skutterudite phase will stop increasing and be constant for a period (first plateau in Fig. 3(b), or blue dashed line in Fig. 1(b)) while the nominal composition is in the Sb-rich three phase region and the resulting skutterudite phase has stable composition (blue point in Fig. 3(a)). This Yb content at which lattice constant stops

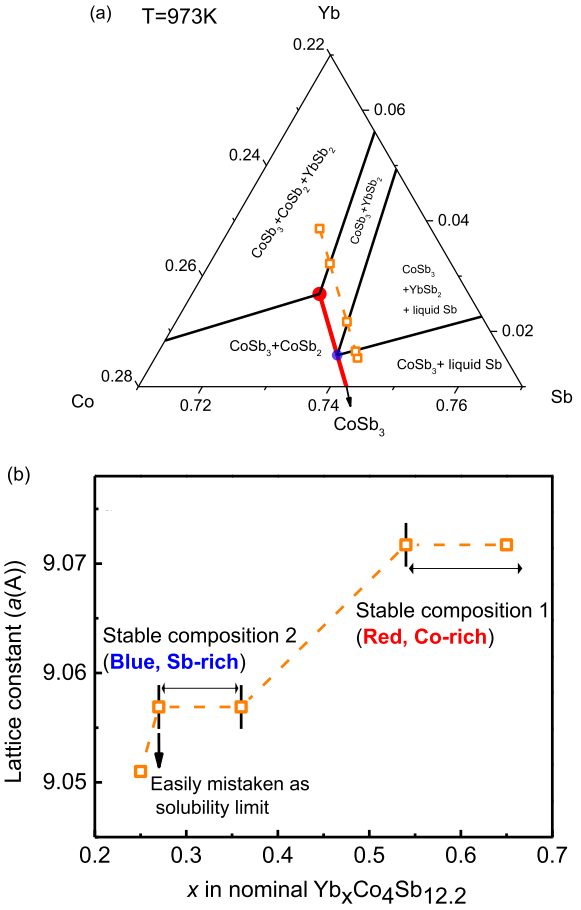

Fig. 3. Samples with different nominal Yb content x in $Yb_xCo_4Sb_{12.2}$ (marked as empty orange rectangles) but the same Sb excess lead to a nonlinear dependence of lattice constant (b) due to the sample traversing different two- and three-phase regions of the phase diagram (a).

increasing can be easily mistaken as the Yb solubility limit [8]. However, as seen from Fig. 3(b), further Yb addition can change the Yb actual content in the skutterudite phase dramatically as the nominal composition moves away from the Sb-rich three phase region and into the two phase region, resuming the lattice constant increase. As the nominal composition moves into the Co-rich three phase region, the actual Yb content reaches the maximum solubility (red point in Fig. 3(a)) and thus the lattice constant reaches a plateau again (second plateau in Fig. 3(b) or red dashed line plateau in Fig. 1(b)). An overall investigation of the phase relations near the targeted phase is thus needed in order to make a conclusion about solubility limit - observing a plateau in lattice constant is insufficient in determining the solubility limit in a ternary system.

3.3. Temperature dependent solubility limit

The partial filling of Yb in the void site increases the entropy due to the increase of disorder of the material, and thus it can be expected that the equilibrium solubility should increase measurably with temperature [7]. In order to study the temperature dependence of these stable skutterudite compositions,

similar methodology was used except samples were annealed at different temperatures, ranging from 773 K to 1073 K (Fig. 11).

Indeed, the Yb solubility of the Co and Sb rich 3-phase regions (red and blue points in Fig. 3(a) respectively) increases significantly with temperature as shown in Fig. 4. The maximum solubility of Yb (red line) increases to about 0.49 ± 0.02 at 1073 K which is about 5 times higher than that at 773 K (0.11 ± 0.02). Note that there is a physical limit of the maximum solubility that one skutterudite unit cell can host "at most" two guest atoms so x should be no more than 1 at any temperature in $R_xCo_4Sb_{12}$.

This variability in Yb solubility, both from annealing temperature and Co/Sb ratio described above, can easily account for differences reported in the literature [5,8,11].

3.4. Thermoelectric properties of optimized compositions

From the analysis of the temperature dependent phase diagram we can predict that the Yb content in the skutterudite phase can be controlled through the annealing temperature when the nominal composition is in one of the three phase regions, either in the Co-rich three phase region of $Yb_xCo_4Sb_{12}$, $CoSb_2$ and $YbSb_2$ or in the Sb-rich three phase region of $Yb_xCo_4Sb_{12}$, $YbSb_2$ and liquid Sb. According to a previous literature study and our unpublished work, the thermoelectric properties can be optimized when the filling fraction x of Yb in $Yb_xCo_4Sb_{12}$ is about 0.2–0.3 [3–5]. From Figs. 4 and 11(a) we can see that when nominal compositions (red open symbols) are in the Co-rich three phase region of $Yb_xCo_4Sb_{12}$, $CoSb_2$ and $YbSb_2$ with an annealing temperature at 873 K, the Yb actual content in skutterudite phase is about $x = 0.3$, so a set of samples with nominal compositions $Yb_xCo_4Sb_{12+y}$ ($x = 0.30, 0.33, 0.36, 0.40$ with $y = 0$) were prepared for thermoelectric evaluation (red data in Figs. 5 and 6). From Figs. 4 and 11(c) we can also see that when nominal compositions (blue open symbols) are in the Sb-rich three phase region of $Yb_xCo_4Sb_{12}$, $YbSb_2$ and liquid Sb, with the annealing temperature as 1023 K, the Yb actual content in skutterudite phase is also about $x = 0.3$, so another sample with nominal composition $Yb_xCo_4Sb_{12+y}$ ($x = 0.33$ with $y = 0.20$) was also prepared (blue data in Figs. 5 and 6). In order to minimize the influence of secondary phases on the thermoelectric properties, nominal compositions were chosen to be very close to the stable points and due to the lever rule, the amount of secondary phases is small and their effect can thus be neglected. For small amounts of secondary phases, it can be shown using effective medium theory that the first order effect on electrical and thermal transport properties is proportional to the volume fraction of impurity [20]. Thus for 1% volume fraction the measured transport properties should only be 1% in error. The temperature dependence of transport properties of these samples are shown in Fig. 5.

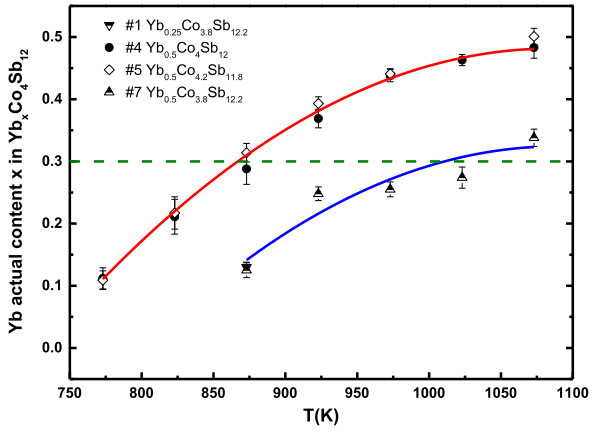

Fig. 4. Temperature dependence of solubility limit of Yb in Yb-doped skutterudites $Yb_xCo_4Sb_{12}$. The red line indicates the temperature dependence of the actual Yb content in the stable skutterudite composition represented as a red point (maximum solubility) in Fig. 3(a). The blue line shows the temperature dependence of the actual Yb content in the stable skutterudite composition represented as a blue point in Fig. 3(a). The dashed green line is the actual Yb content ($x = 0.3$) targeted for optimized thermoelectric properties, which crosses the solubility lines at 873 K and 1023 K respectively.

The temperature dependence of the electrical resistivity and Seebeck coefficient of $Yb_xCo_4Sb_{12+y}$ (nominal $x = 0.33$ with $y = 0.20$; $x = 0.30, 0.33, 0.36, 0.40$ with $y = 0$) is shown in Fig. 5(a) and (b), respectively. All the samples show negative Seebeck coefficients throughout the whole temperature range, indicating the expected n-type semiconductor behaviour. With increasing temperature, both the electrical resistivity and the magnitude of the Seebeck coefficient increase, which is typical behaviour for heavily doped semiconductors. Fig. 5(c) shows the temperature dependence of total thermal conductivity (κ). In the whole temperature range investigated, the total thermal conductivity for all samples is lower than 3.8 $Wm^{-1} K^{-1}$. κ_L is obtained by subtracting the electronic contribution from the total thermal conductivity using the Wiedemann–Franz law. We adopted a Lorentz number of 2.0×10^{-8} $V^2 K^{-2}$ to simplify the estimation of electronic thermal conductivity, and this value is also consistent with the experimentally estimated value based on previous work on skutterudites [21]. All Yb-doped samples show strongly reduced κ_L as compared to binary $CoSb_3$ with κ_L ~10 $Wm^{-1} K^{-1}$ at 300 K. As can be seen from Fig. 5(d), the lattice thermal conductivity at 300 K stops decreasing with the Yb content x when x exceeds 0.33, while the carrier concentration stops increasing with Yb content x when x exceeds 0.36 from Fig. 5(a), both indicating the Yb actual content reaches solubility limit at 873 K when $x \geq 0.36$.

Fig. 6 shows the temperature dependence of dimensionless thermoelectric figure of merit (zT) which is consistent with prior reports from reference 4. The highest zT value in Yb-doped skutterudite samples reaches 1.3 at 850 K with $x = 0.3$. All samples have zT value higher than 1.1 at and above 800 K. This is confirmed for samples targeting both stable compositions with variation in nominal compositions to represent uncertainty in processing. Thus it enables the production of optimized skutterudites at an easily reproducible and commercial scale. The measured zT values follow the trend of reference 4 similar to those in other reports on $Yb_xCo_4Sb_{12}$ [3,5].

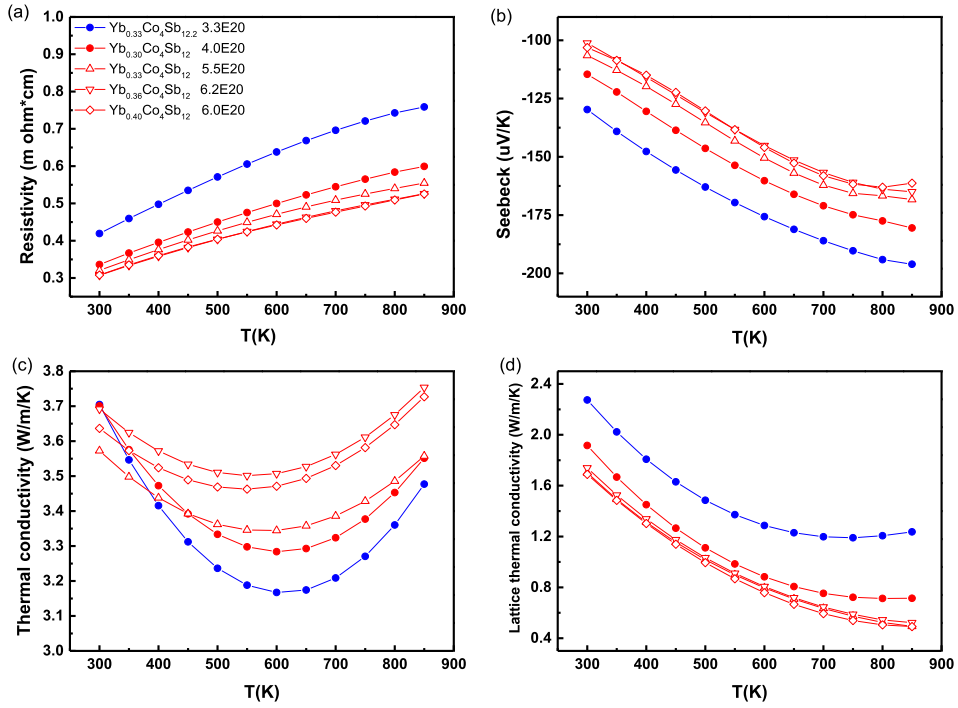

Fig. 5. The temperature dependence of transport properties: (a) electrical resistivity, (b) Seebeck coefficient, (c) thermal conductivity, (d) lattice thermal conductivity of Yb-doped $CoSb_3$ based skutterudites with a Lorentz number of 2.0×10^{-8} V^2 K^{-2}. Numbers in (a) denotes the measured Hall carrier density at 300 K.

3.5. Stability of optimized compositions

The temperature dependent solubility limit predicts the precipitation of impurity phases at intermediate temperature, as shown schematically in Fig. 7. Such temperature dependent solubility and precipitation has been observed in other ternary systems such as Na-doped PbTe as well [22]. In heavily doped SiGe, the precipitation and redissolution of dopants during high-temperature transport measurements was also reported [23]. The rate and size of the precipitates will depend on the temperature and time. As the optimum carrier concentration corresponds to approximately $x = 0.3$, $Yb_{0.3}Co_4Sb_{12}$ material above 873 K will be stable indefinitely. The $Yb_{0.3}Co_4Sb_{12}$ material at low temperatures will be thermodynamically unstable but kinetically stable because precipitation will require the Yb diffusion which will be low at low temperatures. In the intermediate temperature range, some precipitation of impurity phases is expected. Reduction of the Yb content will also reduce the carrier concentration which will raise the electrical resistivity of the material. Despite the formation of impurity phases, the maximum performance of the material may not be dramatically reduced because a lower carrier concentration at low temperature may actually increase the zT at that temperature [24]. Such a temperature dependent doping effect was found in Ag doped n-type PbTe–Ag_2Te nanocomposites to improve the thermoelectric performance [25]. The large difference in solubility limit at different

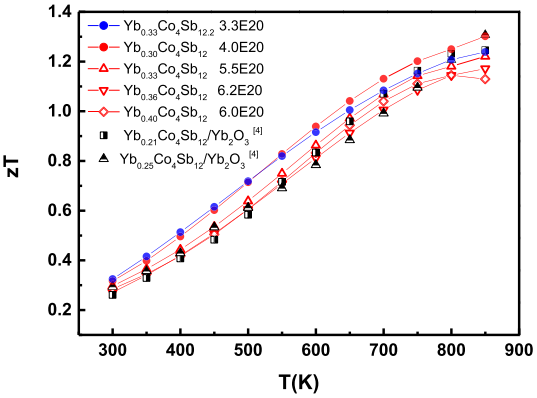

Fig. 6. Temperature dependence of the thermoelectric figure of merit (zT) for Yb-doped skutterudites targeting the same $Yb_xCo_4Sb_{12}$ composition using samples annealed at 873 K without excess Sb (red stable point) and 1023 K with excess Sb (blue stable point).

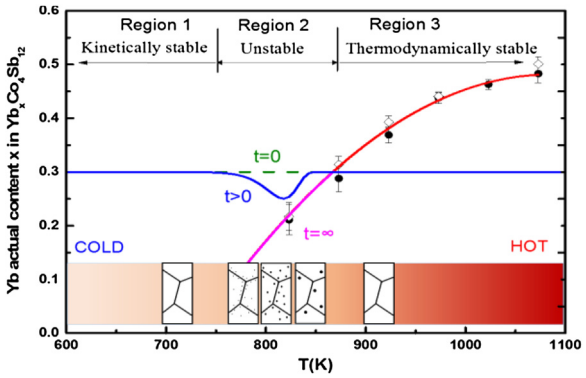

Fig. 7. Stability of $Yb_xCo_4Sb_{12}$ skutterudite with optimum dopant composition $x = 0.3$. During operation (time $t > 0$), dopant precipitation is predicted in region 2 where the skutterudite phase is neither thermodynamically stable (as in region 3) nor kinetically stable (as in region 1).

temperatures could also be used to form nano-scale precipitates with controlled size [26,27].

4. Conclusions

The equilibrium isothermal sections of the ternary phase diagram of Yb–Co–Sb system at various temperatures are studied. XRD, SEM and EPMA analysis indicate that there is a three-phase region on the Co-rich side of Yb-doped skutterudites ($Yb_xCo_4Sb_{12}$, $CoSb_2$ and $YbSb_2$) which results in a stable skutterudite composition $Yb_xCo_4Sb_{12}$ with maximum Yb content (any nominal composition in this three-phase region will produce a skutterudite phase with the same Yb content, for example $x = 0.11 \pm 0.02$ at 773 K and $x = 0.49 \pm 0.02$ at 1073 K), and another three-phase region ($Yb_xCo_4Sb_{12}$, $YbSb_2$ and liquid Sb) on the Sb-rich side with a stable composition $Yb_xCo_4Sb_{12}$ with relatively lower Yb content (for example $x = 0.13 \pm 0.01$ at 873 K and $x = 0.34 \pm 0.01$ at 1073 K). At higher temperatures, the equilibrium Yb content in both stable compositions is also higher, which can be used to form nano-scale precipitates in matrix skutterudite phase. Skutterudite material with the optimized thermoelectric composition can be produced from a range of nominal compositions with appropriate annealing. Figure of merit zT values greater than 1.1 were obtained at and above 800 K in all samples targeting $Yb_xCo_4Sb_{12}$ with $x = 0.3$. The highest zT value reaches 1.3 at 850 K in $Yb_{0.30}Co_4Sb_{12}$.

Supporting materials.

1. Structure characterization

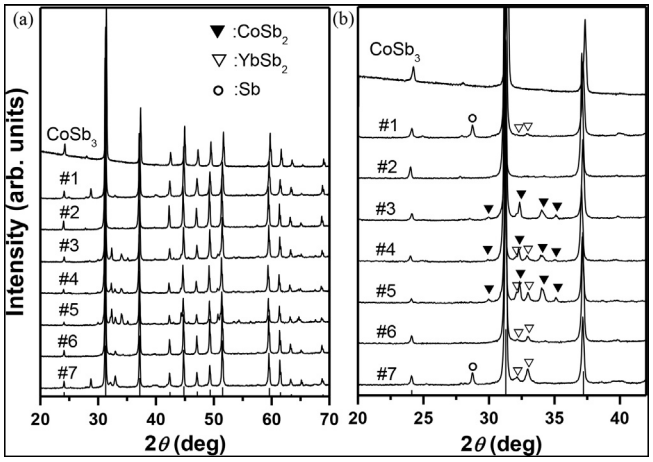

Fig. 8. (a) XRD patterns of undoped $CoSb_3$ and the Yb-doped skutterudites annealed at 973 K with nominal compositions #1 $Yb_{0.25}Co_{3.8}Sb_{12.2}$, #2 $Yb_{0.25}Co_4Sb_{12}$, #3 $Yb_{0.25}Co_{4.2}Sb_{11.8}$, #4 $Yb_{0.5}Co_4Sb_{12}$, #5 $Yb_{0.5}Co_{4.2}Sb_{11.8}$, #6 $Yb_{0.5}Co_{3.9}Sb_{12.1}$, and #7 $Yb_{0.5}Co_{3.8}Sb_{12.2}$. (b) Magnification of the XRD patterns in (a).

Fig. 8(a, b) shows the X-ray diffraction results of Yb-doped skutterudites annealed at 973 K with nominal compositions #1–7. All major diffraction peaks are indexable to the skutterudite phase, as identified using Powder Diffraction File reference number 01-078-0976 for $CoSb_3$ in International Center for Diffraction Data (ICDD). However, except for the pattern of sample #2 $Yb_{0.25}Co_4Sb_{12}$, all the other patterns show impurity phases (secondary phase other than skutterudite phase). Sb (Ref. No. 00-001-0802) and $YbSb_2$ (Ref. No. 01-073-0450) were both found in Sb-rich samples #1 $Yb_{0.25}Co_{3.8}Sb_{12.2}$ and #7 $Yb_{0.5}Co_{3.8}Sb_{12.2}$. $YbSb_2$ alone was found in sample #6 $Yb_{0.5}Co_{3.9}Sb_{12.1}$. $CoSb_2$ alone was found in Co-rich sample with relatively lower Yb content #3 $Yb_{0.25}Co_{4.2}Sb_{11.8}$. Both $CoSb_2$ (Ref. No. 00-029-0126) and $YbSb_2$ were found in samples #4 $Yb_{0.5}Co_4Sb_{12}$ and #5 $Yb_{0.5}Co_{4.2}Sb_{11.8}$ (samples with relatively higher Yb content with/without Co-rich).

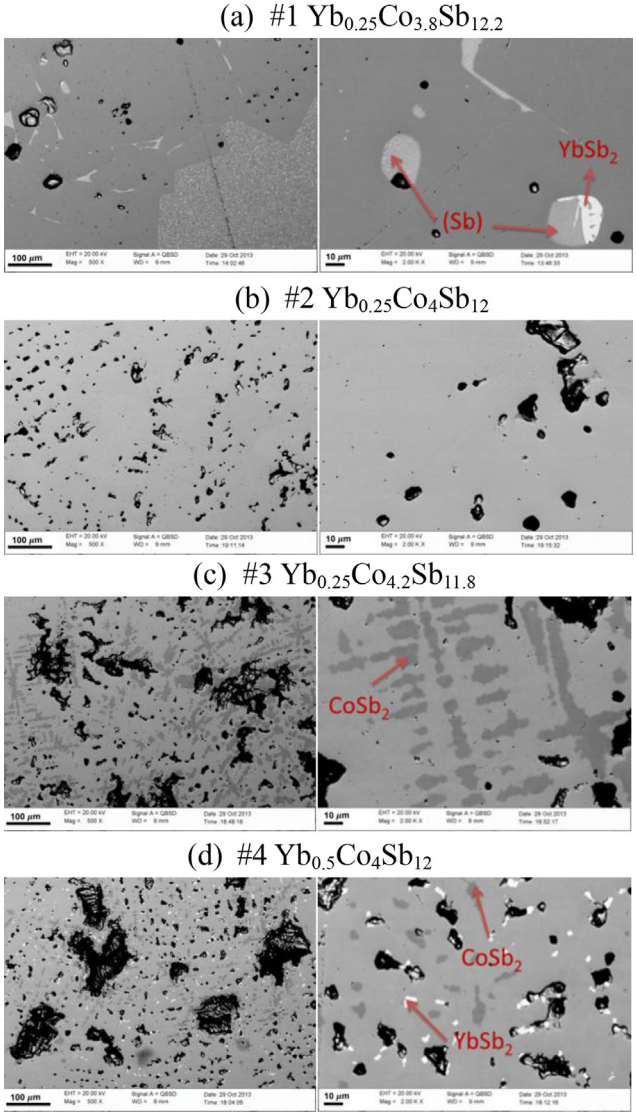

Fig. 9. Scanning electron microscope (SEM) images of samples #1–7 annealed at 973 K. Black regions are holes formed by thermal contraction during quenching.

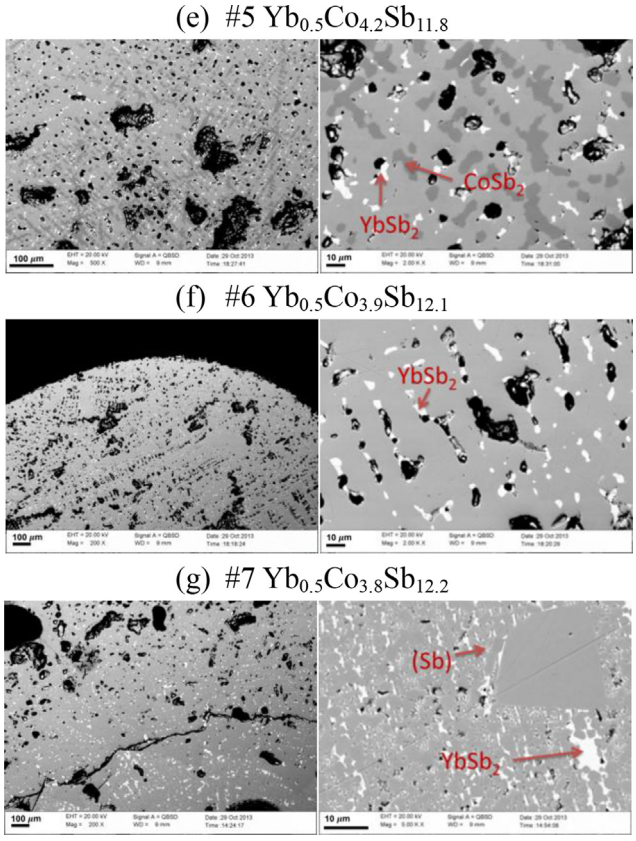

Fig. 9 (*continued*)

Scanning electron microscope (SEM) images were taken for all seven samples annealed at 973 K, as shown in Fig. 9. These results are consistent with our XRD data shown in Fig. 8. Electron probe microanalysis (EPMA) measurements were carried out at ten different locations on the skutterudite phase region and the average Yb contents are listed in Table 1. Note that in sample #3 annealed at 973 K, the actual Yb content in the skutterudite phase ($x = 0.302 \pm 0.010$) is higher than the one in the nominal composition ($x = 0.25$) because there is little Yb solubility in the $CoSb_2$ phase, allowing more Yb to segregate to the $CoSb_3$ phase. This is consistent with the lever rule.

Table 1
Actual Yb content in the skutterudite phase estimated by EPMA for Yb-containing skutterudites with different nominal compositions and annealing temperatures. Boldface Yb contents for sample #4 and #5 correspond to the stable skutterudite composition represented as a red point in Fig. 11. Boldface Yb contents for sample #1 and #7 correspond to the stable skutterudite composition represented as a blue point in Fig. 11.

Samples	Annealing T(K)	EPMA Yb content
#1 $Yb_{0.25}Co_{3.8}Sb_{12.2}$	873	**0.130 ± 0.008**
	923	0.158 ± 0.022
	973	0.192 ± 0.014

Table 1 (*continued*)

Samples	Annealing T(K)	EPMA Yb content
	1023	0.209 ± 0.014
	1073	0.187 ± 0.014
#2 $Yb_{0.25}Co_4Sb_{12}$	973	0.215 ± 0.016
#3 $Yb_{0.25}Co_{4.2}Sb_{11.8}$	973	0.302 ± 0.010
#4 $Yb_{0.5}Co_4Sb_{12}$	773	0.112 ± 0.017
	823	0.211 ± 0.028
	873	**0.288 ± 0.025**
	923	0.369 ± 0.015
	973	**0.438 ± 0.010**
	1023	**0.463 ± 0.009**
	1073	**0.483 ± 0.017**
#5 $Yb_{0.5}Co_{4.2}Sb_{11.8}$	773	0.109 ± 0.015
	823	0.217 ± 0.026
	873	**0.314 ± 0.015**
	923	0.393 ± 0.011
	973	**0.441 ± 0.008**
	1023	**0.384 ± 0.018**
	1073	**0.501 ± 0.013**
#6 $Yb_{0.5}Co_{3.9}Sb_{12.1}$	973	0.260 ± 0.019
#7 $Yb_{0.5}Co_{3.8}Sb_{12.2}$	873	**0.125 ± 0.012**
	923	0.248 ± 0.011
	973	**0.255 ± 0.012**
	1023	**0.274 ± 0.017**
	1073	**0.338 ± 0.014**

2. Phase diagrams at different temperatures

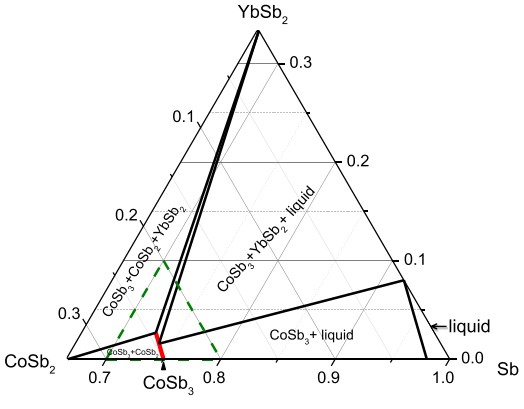

Fig. 10. Proposed phase diagram for Yb-containing skutterudites. The red line indicates the solubility region of Yb in $CoSb_3$. A magnification of the triangle area formed by green dashed lines is shown in Fig. 11 at different temperatures (873 K, 973 K, 1023 K, and 1073 K).

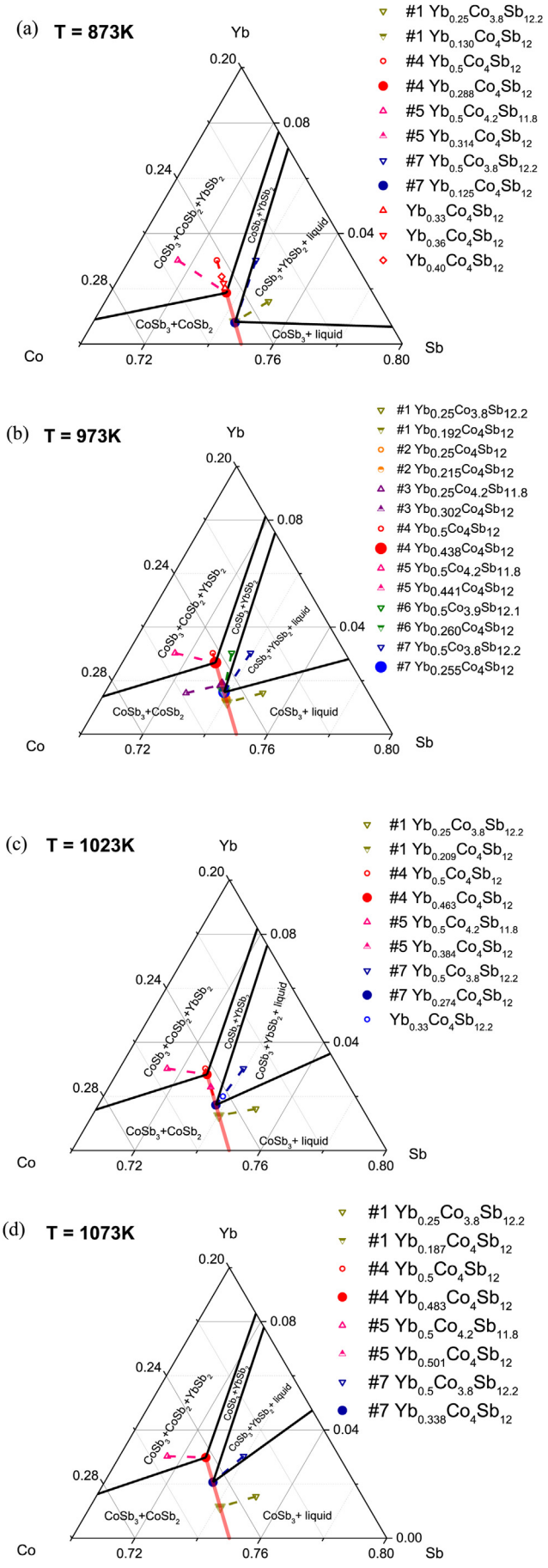

Fig. 11. Magnifications of phase regions near $CoSb_3$ of isothermal sections of Yb-Co-Sb ternary phase diagram system at (a) 873 K, (b) 973 K, (c) 1023 K, and (d) 1073 K. The solid red line indicates the void filling in the direction $(Yb_{VF})_xCo_4Sb_{12}$. The red point represents the stable composition of the skutterudite phase obtained when the nominal composition is in the Co-rich three phase region ($YbSb_2$, $CoSb_2$ and $Yb_xCo_4Sb_{12}$). The blue point represents the stable composition of the skutterudite phase obtained when the nominal composition is in the Sb-rich three phase region ($YbSb_2$, liquid Sb and $Yb_xCo_4Sb_{12}$). The nominal sample compositions are shown as open symbols. Solid symbols represent the composition of the skutterudite majority phase using the experimental EPMA value for Yb content, and positioned on the red line. The nominal (open symbols) and experimental compositions (solid symbols) are connected with a dotted line.

Acknowledgements

The authors acknowledge the financial support of National Science Council of Taiwan (NSC101-3113-P-008-001). We thank Yulong Li, Xun Shi, Lidong Chen of Shanghai Institute of Ceramics, Chinese Academy of Sciences for ZEM-3 measurements.

References

[1] Slack GA. New materials and performance limits for thermoelectric cooling. In: Rowe DM, editor. CRC handbook of thermoelectrics. Florida, USA: CRC Press; 1995. p. 407.
[2] Meisner GP. Presented at directions in engine-efficiency and emissions research, Detroit. October, 2011.
[3] Nolas GS, Kaeser M, Littleton RT, Tritt TM. High figure of merit in partially filled ytterbium skutterudite materials. Appl Phys Lett 2000;77(12):1855–7.
[4] Zhao X, Shi X, Chen L, Zhang W, Bai S, Pei Y, et al. Synthesis of $YbyCo_4Sb_{12}/Yb_2O_3$ composites and their thermoelectric properties. Appl Phys Lett 2006;89(9):092121-1–092121-3.
[5] Li H, Tang X, Zhang Q, Uher C. Rapid preparation method of bulk nanostructured $Yb_{0.3}Co_4Sb_{12}$ compounds and their improved thermoelectric performance. Appl Phys Lett 2008;93(25):252109-1–252109-3.
[6] Mei Z, Zhang W, Chen L, Yang J. Filling fraction limits for rare-earth atoms in $CoSb_3$: an ab initio approach. Phys Rev B 2006;74(15):153202-1–153202-4.
[7] Shi X, Zhang W, Chen L, Yang J, Uher C. Thermodynamic analysis of the filling fraction limits for impurities in $CoSb_3$ based on ab initio calculations. Acta Mater 2008;56(8):1733–40.
[8] Dilley NR, Bauer ED, Maple MB, Sales BC. Thermoelectric properties of chemically substituted skutterudites Yb[sub y]Co[sub 4]Sn[sub x]Sb [sub 12–x]. J Appl Phys 2000;88(4):1948–51.
[9] Xia X, Qiu P, Shi X, Li X, Huang X, Chen L. High- temperature oxidation behavior of filled skutterudites $YbyCo_4Sb_{12}$. J Electron Mater 2012;41(8):2225–31.
[10] Salvador JR, Yang J, Shi X, Wang H, Wereszczak AA, Kong H, et al. Transport and mechanical properties of Yb-filled skutterudites. Philos Mag 2009;89(19):1517–34.
[11] Yang J, Hao Q, Wang H, Lan Y, He Q, Minnich A, et al. Solubility study of Yb in n-type skutterudites $YbxCo_4Sb_{12}$ and their enhanced thermoelectric properties. Phys Rev B 2009;80(11):115329-1–115329-5.
[12] Qiu Y, Xi L, Shi X, Qiu P, Zhang W, Chen L, et al. Charge-compensated compound defects in Ga-containing thermoelectric skutterudites. Adv Funct Mater 2013;23(25):3194–203.
[13] Tang Y, Qiu Y, Xi L, Shi X, Zhang W, Chen L, et al. Phase diagram of In–Co–Sb system and thermoelectric properties of In-containing skutterudites. Energy Environ Sci 2014;7(2):812–9.
[14] Okamoto H. Co–Sb. J Phase Equilib 1991;12:244–5.

[15] Okamoto H. Sb–Yb (Antimony–Ytterbium). In: Massalski TB, Okamoto H, editors. Binary Alloy phase diagrams. II ed., vol. 3. Asm Intl; 1990. p. 3317–20.
[16] Okamoto H. Co–Yb (Cobalt–Ytterbium). In: Massalski TB, Okamoto H, editors. Binary Alloy phase diagrams. II ed., vol. 3. Asm Intl; 1990. p. 1261–2.
[17] LaLonde AD, Ikeda T, Snyder GJ. Rapid consolidation of powdered materials by induction hot pressing. Rev Sci Instrum Feb 2011;82(2):025104-1–025104-4.
[18] Borup KA, Toberer ES, Zoltan LD, Nakatsukasa G, Errico M, Fleurial JP, et al. Measurement of the electrical resistivity and Hall coefficient at high temperatures. Rev Sci Instrum Dec 2012;83(12):123902-1–123902-7.
[19] Lamberton GA, Tedstrom RH, Tritt TM, Nolas GS. Thermoelectric properties of Yb-filled Ge-compensated CoSb[sub 3] skutterudite materials. J Appl Phys 2005;97(11):113715-1–113715-5.
[20] Day TW, Zeier WG, Brown DR, Melot BC, Snyder GJ. Determining conductivity and mobility values of individual components in multiphase composite $Cu_{1.97}Ag_{0.03}Se$. Appl Phys Lett 2014;105(17):172103-1–172103-5.
[21] Shi X, Yang J, Salvador JR, Chi M, Cho JY, Wang H, et al. Multiple-filled skutterudites: high thermoelectric figure of merit through separately optimizing electrical and thermal transports. J Am Chem Soc May 25 2011;133(20):7837–46.
[22] Aminorroaya-Yamini S, Ikeda T, Lalonde A, Pei Y, Dou SX, Snyder GJ. Rational design of p-type thermoelectric PbTe: temperature dependent sodium solubility. J Mater Chem A 2013;1:8725–30.
[23] Vining CB. A model for the high-temperature transport properties of heavily doped n-type silicon–germanium alloys. J Appl Phys 1991;69(1):331–41.
[24] Snyder GJ, Toberer ES. Complex thermoelectric materials. Nat Mater 2008;7:105–14.
[25] Pei Y, May AF, Snyder GJ. Self-tuning the carrier concentration of PbTe/Ag_2Te composites with excess Ag for high thermoelectric performance. Adv Energy Mater 2011;1(2):291–6.
[26] Ikeda T, Ravi V, Snyder G. Formation of Sb_2Te_3 Widmanstätten precipitates in thermoelectric PbTe. Acta Mater 2009;57(3):666–72.
[27] Heinz NA, Ikeda T, Pei Y, Snyder GJ. Applying quantitative microstructure control in advanced functional composites. Adv Funct Mater 2014;24(15):2135–53.

Yinglu Tang is a graduate student in the Materials Science Department at Caltech. Yinglu got her Bachelor's degree of Science in the Materials Science and Engineering Department at Beihang University in 2008 and Engineering degree in Mechanical Engineering at Arts et Metiers ParisTech in 2010 before joining Caltech. Her current research focuses on the formation and optimization of skutterudite thermoelectric materials using phase diagrams.

Jeff Snyder is professor of Materials Science and Engineering at Northwestern University. He is also a Faculty Associate in the Materials Science Department at Caltech and a Visiting Professor at SKKU University Korea, ITMO University Saint Petersburg, Wuhan University of Technology and the Shanghai Institute of Ceramics - Chinese Academy of Sciences. He was a Senior Member of the Technical Staff in the thermoelectrics group at JPL for 9 years (1997–2006). Dr. Snyder has over 200 publications on thermoelectric materials, devices and applications. Dr. Snyder is also a board member and Treasurer for the International Thermoelectric Society.